Multiscale Model for Turbulent Flows

David C. Wilcox*
DCW Industries, Inc., La Cañada, California

A model is devised for computing general turbulent flows. The model is an improvement over two-equation turbulence models in a critically important manner, that is, the new model accounts for disalignment of the Reynolds-stress-tensor and the mean-strain-rate-tensor principal axes. The improved representation of the Reynolds-stress tensor has been accomplished through the introduction of a multiscale description of the turbulence, i.e., two energy scales are used corresponding to upper and lower partitions of the turbulence energy spectrum. A novel feature of the formulation is that the differential equation for the Reynolds-stress tensor is of first order, which in effect corresponds to what can be termed an "algebraic stress model" with convective terms. As a consequence of its mathematical simplicity, the model is very efficient and easy to implement computationally. The model is applied to a wide range of turbulent flows including homogeneous turbulence, compressible and incompressible two-dimensional boundary layers, and unsteady boundary layers including periodic separation and reattachment. Comparisons with corresponding experimental data show that the model reproduces all salient features of the flows considered. Perturbation analysis of the viscous sublayer shows that integration through the sublayer can be accomplished with no special viscous modifications to the closure coefficients appearing in the model.

I. Introduction

THIS paper presents results of the second phase of a continuing turbulence-modeling effort initiated after the second Stanford conference[1] on turbulent flows. The first phase led to development of a new two-equation turbulence model[2] that is much more accurate than any existing model for boundary layers in an adverse pressure gradient. In this phase, the primary goal is to focus on the constitutive relation between Reynolds stress and mean-flow properties.

An important shortcoming of two-equation turbulence models is their inability to adjust at physically realistic rates to a change in the mean-strain-rate tensor field. This shortcoming is most easily seen by examining two-equation model predictions for homogeneous turbulence in uniform shear, such as the flow considered by Champagne et al.[3] Wilcox and Rubesin[4] have shown that a two-equation model predicts an asymptotic approach to the experimentally measured asymptotic structure to within experimental accuracy. However, the predicted time to reach the asymptote is an order of magnitude longer than measured. This shortcoming is a direct consequence of the two-equation model's assumption that Reynolds stress is proportional to mean-strain rate.

Another straightforward example of this shortcoming is provided by a homogeneous turbulence that has been subjected for some time to a uniform rate of strain, followed by sudden removal of the strain rate. As shown in many experiments, the turbulence approaches isotropy asymptotically with time. However, if we postulate that Reynolds stress is proportional to mean-strain rate, the model will predict an instantaneous return to isotropy. Note that the same conclusion holds for nonlinear stress/strain-rate constitutive relationships, such as the so-called algebraic stress model.

Presented as Paper 86-0029 at the AIAA 24th Aerospace Sciences Meeting, Reno, NV, Jan. 6-9, 1986, and Paper 87-0290 at the AIAA 25th Aerospace Sciences Meeting, Reno, NV, Jan. 12-15, 1987; received Jan. 29, 1987; revision received Dec. 21, 1987.

*President. Associate Fellow AIAA.

To overcome this shortcoming, some researchers have attempted to develop a model for the Reynolds-stress tensor equation obtained by taking moments of the Navier-Stokes equation. The drastic surgery performed in such attempts often leaves rigor far behind and, in effect, appears more as an attempt to model the differential equations rather than the physics of turbulent flow processes. In this study, a deliberate attempt has been made to avoid the conventional approach. Thus, although the final set of equations formulated in this paper shares many features of models devised by others, the approach taken differs both in detail and in spirit.

There have been two key developments that have stimulated the approach taken in this paper. The first is the development of the algebraic stress model by Rodi[5] and subsequently exercised in many applications by Lakshminarayana.[6] Using the algebraic stress model yields an accurate method for describing effects of streamline curvature and secondary motions, for example, two effects that cannot be directly represented with a standard two-equation turbulence model. The second development is the elegant Johnson-King[7] model. This model implements a simple first-order differential equation for shear-stress magnitude to be used in conjunction with the mixing-length model in order to circumvent shortcomings of the mixing-length model in separated flows. The goals of this study are to 1) create a model similar to the algebraic stress model, which also accounts for sudden changes in mean-strain rate, and 2) create a complete tensor-invariant analog of the Johnson-King model in the context of advanced turbulence models.

In this paper, we begin with the premise that turbulence can be described by representing the turbulence energy spectrum in terms of an upper and a lower partition with the upper partition corresponding to lowest frequency, energy-bearing eddies. This notion is used in large-eddy simulation work[8] where small eddies (corresponding to the lower partition of the spectrum) are modeled and large eddies (corresponding to the upper partition of the spectrum) are numerically simulated. By contrast, we model both the small and the large eddies. We use the general observations[9] that eddies in the lower partition are expected to contain most of the vorticity, to be isotropic, and to dissipate rapidly into heat. A key feature of eddies in the upper partition is that they are more or less inviscid. As shown in Sec. III, in terms of model equations these facts yield 1) two

equations that are essentially the two-equation model devised by Wilcox,[2] and 2) an inviscid tensor equation for the upper partition contribution to the Reynolds-stress tensor.

After stating the complete multiscale model equations in Sec. II, closure approximations are discussed in detail in Sec. III. In special limiting cases, some of the approximations are similar to those introduced by Launder et al.[10] All closure coefficients that the multiscale model has in common with the Wilcox k-ω model[2] assume the same values used in the two-equation model. Values for all additional closure coefficients are selected based on general observations of turbulent flow behavior, perturbation analysis of the viscous sublayer, and a modest amount of computer optimization. Section IV presents results of numerical applications to homogeneous turbulent flows. Section V summarizes results of a perturbation analysis of model-predicted viscous sublayer structure. Section VI presents three types of numerical applications including steady incompressible turbulent boundary layers, steady compressible turbulent boundary layers, and unsteady incompressible turbulent boundary layers. In all cases, comparisons with experimental data are presented.

II. Equations of Motion

Before proceeding to develop the multiscale model, it is instructive to first summarize the complete set of equations that constitute the model. For general compressible turbulent fluid flows, the turbulence model equations are written in terms of Favre[11] mass-averaged quantities as follows:

Mass conservation:

$$\frac{\partial \rho}{\partial t} + \frac{\partial}{\partial x_j}(\rho u_j) = 0 \tag{1}$$

Momentum conservation:

$$\frac{\partial}{\partial t}(\rho u_i) + \frac{\partial}{\partial x_j}(\rho u_j u_i) = -\frac{\partial p}{\partial x_i} + \frac{\partial \hat{\tau}_{ji}}{\partial x_j} \tag{2}$$

Mean energy Conservation:

$$\frac{\partial}{\partial t}(\rho E) + \frac{\partial}{\partial x_j}(\rho u_j H) = \frac{\partial}{\partial x_j}\left[u_i \hat{\tau}_{ij} + (\mu + \sigma^* \mu_T)\frac{\partial k}{\partial x_j} - q_j\right] \tag{3}$$

Turbulent kinetic energy:

$$\frac{\partial}{\partial t}(\rho k) + \frac{\partial}{\partial x_j}(\rho u_j k) = \tau_{ij}\frac{\partial u_i}{\partial x_j} - \beta^* \rho \omega k + \frac{\partial}{\partial x_j}\left[(\mu + \sigma^* \mu_T)\frac{\partial k}{\partial x_j}\right] \tag{4}$$

Specific dissipation rate:

$$\frac{\partial}{\partial t}(\rho \omega) + \frac{\partial}{\partial x_j}(\rho u_j \omega) = \left(\frac{\gamma \omega}{k}\right)\tau_{ij}\frac{\partial u_i}{\partial x_j} - \beta \rho \omega^2 - \xi \beta \rho \omega \sqrt{2\Omega_{mn}\Omega_{nm}} + \frac{\partial}{\partial x_j}\left[(\mu + \sigma \mu_T)\frac{\partial \omega}{\partial x_j}\right] \tag{5}$$

Upper partition stress tensor:

$$\frac{\partial}{\partial t}(\rho T_{ij}) + \frac{\partial}{\partial x_k}(\rho u_k T_{ij}) = -P_{ij} + E_{ij} \tag{6}$$

where t is time, x_i is position vector, u_i is velocity vector, ρ is density, p is pressure, μ is molecular viscosity, $\hat{\tau}_{ij}$ is the sum of the molecular and Reynolds stress tensors, and q_j is the sum of the molecular and turbulent heat flux vectors. In Eq. (3), the quantities $E = \epsilon + k + u_i u_i/2$ and $H = h + k + u_i u_i/2$ are total energy and enthalpy, respectively, with $h = \epsilon + p/\rho$; ϵ and h denote internal energy and enthalpy. Additionally, τ_{ij} is the Reynolds-stress tensor. The turbulent kinetic energy k and the specific dissipation rate ω are needed to define the eddy viscosity μ_T, which is given by

$$\mu_T = \rho k/\omega \tag{7}$$

The total viscous stress tensor is given by

$$\hat{\tau}_{ij} = 2\mu\left[S_{ij} - \left(\frac{1}{3}\right)\left(\frac{\partial u_k}{\partial x_k}\right)\delta_{ij}\right] + \tau_{ij} \tag{8}$$

where, by definition, the mean-strain-rate tensor S_{ij} and the mean-rotation tensor Ω_{ij} [appearing in Eq. (5)] are given by

$$S_{ij} = \frac{1}{2}\left(\frac{\partial u_i}{\partial x_j} + \frac{\partial u_j}{\partial x_i}\right) \tag{9a}$$

$$\Omega_{ij} = \frac{1}{2}\left(\frac{\partial u_i}{\partial x_j} - \frac{\partial u_j}{\partial x_i}\right) \tag{9b}$$

The heat flux vector q_j is approximated as

$$q_j = -\left(\frac{\mu}{Pr_L} + \frac{\mu_T}{Pr_T}\right)\frac{\partial h}{\partial x_j} \tag{10}$$

where Pr_L and Pr_T are the laminar and turbulent Prandtl numbers, respectively.

In order to close this system of equations, we must postulate a relation between the Reynolds stress tensor τ_{ij} and mass-averaged flow properties. The multiscale model computes τ_{ij} according to

$$\tau_{ij} = \rho T_{ij} - \tfrac{2}{3}\rho e \delta_{ij} \tag{11}$$

where ρT_{ij} is the upper partition contribution to the Reynolds-stress tensor and ρe is the energy of the eddies in the lower partition. The tensor E_{ij} in Eq. (6) represents the exchange of energy among the mean, upper, and lower partition energies and is given by

$$E_{ij} = -C_1 \beta^* \omega\left(\tau_{ij} + \frac{2}{3}\rho k \delta_{ij}\right) + \hat{\alpha} P_{ij} + \hat{\beta} D_{ij} + \hat{\gamma}\rho k\left(S_{ij} - \frac{1}{3}\frac{\partial u_k}{\partial x_k}\delta_{ij}\right) + \frac{2}{3}\rho \omega k (1 - e/k)^{3/2}\delta_{ij} \tag{12}$$

The tensors P_{ij} and D_{ij} are the conventional production tensors defined by

$$P_{ij} = \tau_{im}\frac{\partial u_j}{\partial x_m} + \tau_{jm}\frac{\partial u_i}{\partial x_m} \tag{13a}$$

$$D_{ij} = \tau_{im}\frac{\partial u_m}{\partial x_j} + \tau_{jm}\frac{\partial u_m}{\partial x_i} \tag{13b}$$

Finally, the 10 closure coefficients appearing in Eqs. (1–12) are as follows.

$$\hat{\alpha} = 42/55, \quad \hat{\beta} = 6/55, \quad \hat{\gamma} = 1/4$$

$$\beta = 3/40, \quad \gamma = 4/5, \quad \sigma = 1/2$$

$$\beta^* = 9/100, \quad \xi = 1, \quad \sigma^* = 1/2$$

$$C_1 = 1 + 4(1 - e/k)^{3/2} \tag{14}$$

III. Theoretical Formulation of the Model

For the sake of clarity, formulation of the multiscale model is done for incompressible flow. The most noteworthy feature of the multiscale model is the idea that we must keep track of energy in two separate partitions of the turbulence energy spectrum. In this spirit, the lower partition of the spectrum is postulated to be responsible for the equilibrium value of the Reynolds-stress tensor, whereas the upper partition gives rise to departure from equilibrium. In formulating the model, special care has been taken in 1) tracing energy transfer between the mean, upper, and lower partition energies, 2) modeling as much of the physics of turbulence as possible within a phenomenological point of view, 3) achieving consistency with conventional closure approximations in special limiting cases, and 4) devising a set of equations that are numerically tractable.

A. Basic Postulates

We begin with the premise that turbulence can be described in terms of the energies of two separate partitions of the turbulence energy spectrum. We also make use of the general observations that eddies in the lower partition are expected to contain most of the vorticity, to be isotropic, and to dissipate rapidly into heat, whereas the eddies in the upper partition are inviscid. In terms of model equations, these facts are stated as follows.

B. Mathematical Decomposition

For incompressible flows, the Reynolds-stress tensor $\tau_{ij} = -\rho \overline{u_i' u_j'}$, where the overbar denotes mass average, is represented as the sum of two contributions,

$$\tau_{ij} = \rho T_{ij} + \rho t_{ij} \tag{15}$$

where T_{ij} and t_{ij} are attributed to the upper and lower partitions, respectively. Assuming the eddies in the upper partition are inviscid, the tensor T_{ij} will change as a result of work done against the mean-velocity gradient field and energy exchange with the eddies in the lower partition. Mathematically, we state these facts by writing

$$\rho \frac{\mathrm{d}T_{ij}}{\mathrm{d}t} = -P_{ij} + E_{ij} \tag{16}$$

where $\mathrm{d}/\mathrm{d}t = \partial/\partial t + u_k \partial/\partial x_k$. The tensor P_{ij} is the production tensor defined in Eq. (13a), and E_{ij} is the energy exchange tensor. Assuming the eddies in the lower partition are isotropic, we can say

$$t_{ij} = -\tfrac{2}{3} e \delta_{ij} \tag{17}$$

where the quantity e represents the energy of the eddies in the lower partition. The equation for e can be written as

$$\rho \frac{\mathrm{d}e}{\mathrm{d}t} = E - D + F \tag{18}$$

where F is diffusion, D is dissipation, and E is the trace of E_{ij}, i.e.,

$$E = \tfrac{1}{2} E_{mm} \tag{19}$$

The total kinetic energy of the turbulent fluctuations k is expressed by contracting the Reynolds-stress tensor so that, in terms of e and T_{ij},

$$k = e - \tfrac{1}{2} T_{mm} \tag{20}$$

Hence, contracting Eq. (16) and combining with Eqs. (18–20), we obtain the following equation for k:

$$\rho \frac{\mathrm{d}k}{\mathrm{d}t} = P - D + F \tag{21}$$

where the "production" term P is the trace of the production tensor, i.e.,

$$P = \tfrac{1}{2} P_{mm} \tag{22}$$

C. Closure Approximation

In order to close the system, we must establish mathematical approximations for the dissipation D, diffusion F, and the energy exchange tensor E_{ij}. To maintain consistency with the Wilcox[2] k-ω model formulation, we express the dissipation and diffusion terms according to

$$D = \beta^* \rho \omega k \tag{23a}$$

$$F = \frac{\partial}{\partial x_j}\left[(\mu + \sigma^* \mu_T)\frac{\partial k}{\partial x_j}\right] \tag{23b}$$

where σ^* is a closure coefficient.

Thus, the remaining task is to establish a rational representation for the energy transfer tensor. We do this in two steps. First, we examine the decay of homogeneous turbulence in the absence of mean velocity gradients. Then, we examine the limiting case of a constant-pressure boundary layer.

In the first step of this procedure, we thus focus on homogeneous turbulence with all mean-velocity gradients set to zero. For such turbulence, the equations for total turbulence kinetic energy and for the energy of the upper partition eddies (k-e) are given by

$$\rho \frac{\mathrm{d}k}{\mathrm{d}t} = -D \tag{24a}$$

$$\rho \frac{\mathrm{d}(k\text{-}e)}{\mathrm{d}t} = -E \tag{24b}$$

Now, if we define the characteristic length scale of the turbulence by

$$\ell = \frac{k^{1/2}}{\omega} \tag{25}$$

then we can rewrite the equation for k as follows:

$$\frac{\mathrm{d}k}{\mathrm{d}t} = -\frac{\beta^* k^{3/2}}{\ell} \tag{26}$$

We now postulate that the large eddies decay on the same scale as the overall turbulence, so that we expect to have

$$\frac{\mathrm{d}(k\text{-}e)}{\mathrm{d}t} = -\frac{\beta^*(k\text{-}e)^{3/2}}{\ell} = -\beta^* \omega k \left(1 - \frac{e}{k}\right)^{3/2} \tag{27}$$

Thus, in the absence of mean velocity gradients, we postulate that the limiting form of E is given by

$$E = \beta^* \rho \omega k \left(1 - \frac{e}{k}\right)^{3/2} \qquad \text{for } S_{ij} = 0 \tag{28}$$

In the second step of the procedure, note that we can combine the lower and upper partition equations to derive an equation for the Reynolds-stress tensor. The equation assumes the following form:

$$\frac{\mathrm{d}\tau_{ij}}{\mathrm{d}t} = -P_{ij} + \tfrac{2}{3}\beta^* \rho \omega k \delta_{ij} + \left(E_{ij} - \tfrac{2}{3} E \delta_{ij}\right) + (\text{diffusion terms}) \tag{29}$$

Equation (29) matches the Launder et al.[10] closure approximation and is consistent with Eq. (28), provided we select

$$E_{ij} = -C_1\beta^*\omega(\tau_{ij} + \tfrac{2}{3}\rho k\delta_{ij}) + \hat{\alpha}P_{ij} + \hat{\beta}D_{ij} + \hat{\gamma}\rho kS_{ij} + \tfrac{2}{3}\beta^*\rho\omega k\left(1 - \frac{e}{k}\right)^{3/2}\delta_{ij} \tag{30}$$

where C_1, $\hat{\alpha}$, $\hat{\beta}$, and $\hat{\gamma}$ are additional closure coefficients, and D_{ij} is defined in Eq. (13b).

D. Specific Dissipation-Rate Equaiton

One additional equation is needed to close the system, namely, an equation for the specific dissipation rate ω. Again, we draw from the earlier work on the two-equation model[2] and an interesting development extracted from the large-eddy simulation work of Bardina et al.[8] The postulated equation for ω is

$$\rho\frac{d\omega}{dt} = \left(\frac{\gamma\omega}{k}\right)P - \beta\rho\omega^2 - \xi\beta\rho\omega\sqrt{2\Omega_{mn}\Omega_{nm}} + \frac{\partial}{\partial x_j}\left[(\mu + \sigma\mu_T)\frac{\partial\omega}{\partial x_j}\right] \tag{31}$$

where β, γ, ξ, and σ are closure coefficients.

The term proportional to ξ follows the work of Bardina et al.[8] In the context of homogeneous turbulence, it is required in order to accurately simulate effects of system rotation. The term also introduces subtle differences between model-predicted effects of plane strain and uniform shear on homogeneous turbulence.

E. Closure Coefficients

The model contains a total of 10 closure coefficients: β, β^*, γ, σ, σ^*, ξ, C_1, $\hat{\alpha}$, $\hat{\beta}$, and $\hat{\gamma}$. We use arguments similar to those presented by Wilcox[2] and in addition we have gone through a very careful series of computations to establish the value of each. Note that, consistent with the notions that most of the vorticity is contained in the lower partition eddies, and that ω is closely related to the fluctuating vorticity, we expect that the four coefficients appearing in Eq. (31) must be independent of the ratio of e to k. After more than 30 applications of this model, we find that only C_1 needs to depend on e/k, and it does so in a straightforward manner. To complete the formulation, a relationship between C_1 and the ratio of e to k must be established. That C_1 should depend upon this ratio seems logical for the following reasons. The mathematical representation of turbulence adopted for this model includes two distinct energy scales. Additionally, inspection of Eqs. (29) and (30) shows that the term proportional to C_1 represents the rate at which anisotropic turbulence returns to isotropy. The process of returning to isotropy should involve interaction of the turbulence with itself, with no net change in total energy of the turbulence. Thus, the only energy scales relevant in such a process would be e and k. Assuming no other dimensional parameters are pertinent (e.g., viscosity), then the only dimensionless grouping available is e/k.

Experimental observations[12] indicate that large eddies tend toward isotropy more rapidly than small eddies. Then, if we rewrite the return-to-isotropy term as

$$C_1\beta^*\omega[\tau_{ij}/\rho + \tfrac{2}{3}k\delta_{ij}] = C_1\epsilon_{\text{tot}}[\tau_{ij}/(\rho k) + \tfrac{2}{3}\delta_{ij}] \tag{32}$$

where $\epsilon_{\text{tot}} = \beta^*\omega k$ appears in the turbulent energy equation, a plausible approximation is to say

$$C_1\epsilon_{\text{tot}} = C_{1L}\epsilon_L + C_{1S}\epsilon_S \tag{33}$$

where ϵ_L and ϵ_S are the dissipation terms appearing in the equations for the upper partition energy (k-e) and the lower partition energy e, respectively. Straightforward manipulation of Eqs. (26), (27), and (33) yields

$$C_1 = C_{1L}\left(1 - \frac{e}{k}\right)^{3/2} + C_{1S}\left[1 - \left(1 - \frac{e}{k}\right)^{3/2}\right] \tag{34}$$

In the limiting case where only small eddies are present, i.e., the limiting case $e \to k$, we expect C_1 to asymptotically approach its smallest physically acceptable value of unity. (If C_1 were smaller than one, anisotropic turbulence would depart further from isotropy.) Thus,

$$C_{1S} = 1 \tag{35}$$

In order to establish the value of C_{1L}, we turn now to analysis of the so-called wall layer. The wall layer is the region of a constant-pressure boundary layer sufficiently close to the surface that convective terms are negligible, yet sufficiently distant from the surface that effects of molecular viscosity are negligible. In the wall layer, the velocity follows the classical law of the wall. Perturbation analysis of the multiscale model shows that convective terms are negligible and, to leading order, the diffusion term in the turbulent energy equation is negligible. From these observations there follows immediately

$$e/k = 1 - (1 - \hat{\alpha} - \hat{\beta})^{2/3} \doteq 3/4 \tag{36}$$

in the wall layer. Then, insisting that the value of C_1 for the wall layer match the value used by Launder et al.,[10] namely, 3/2, there follows

$$C_{1L} = 5 \tag{37}$$

Thus, the final form for C_1 postulated for the multiscale model is given by

$$C_1 = 1 + 4\left(1 - \frac{e}{k}\right)^{3/2} \tag{38}$$

In summary, the closure coefficients for the multiscale model are given in Eqs. (14). All applications in the following sections have been done using these values for the closure coefficients.

F. Discussion

Before proceeding to the applications, it is worthwhile to pause and discuss some of the premises underlying formulation of the multiscale model. A novel feature of the model is that it uses a single turbulence-length-scale determining equation. This is a direct consequence of the assumption that upper partition eddies decay on the same scale as the overall turbulence, as reflected in Eq. (27). This approximation has been, to some extent, substantiated by large-eddy simulation studies.[8] Given the uncertainties surrounding proper modeling of the length-scale-determining equation, introducing this approximation is neither more nor less rigorous than adding a second length-scale determining equation. Note that this means the model equations implicitly (and automatically) determine the boundary between the lower and upper partitions of the energy spectrum.

The most controversial approximation made is that the lower partition eddies are isotropic. To explain why, we first contract Eq. (6) to form the following equation for the upper partition turbulent energy:

$$\rho\frac{d(k\text{-}e)}{dt} = (1 - \hat{\alpha} - \hat{\beta})P - \beta^*\rho\omega k\left(1 - \frac{e}{k}\right)^{3/2} \tag{39}$$

Because we have used the Launder-Reece-Rodi values for $\hat{\alpha}$ and $\hat{\beta}$, the value of $(1 - \hat{\alpha} - \hat{\beta})$ is approximately 0.13. Consequently, only 13% of the total turbulence energy production goes into the upper partition. Thus, we should expect that the lower partition energy will often be a significant fraction of

the total. In the wall layer, for example, the ratio e/k is 0.75. This means that the boundary between energy partitions will often lie above the inertial subrange, encroaching on the energy-containing eddies, which are certainly not isotropic. Although postulating that eddies this far up the spectrum are isotropic may be physically unrealistic, the mathematical simplification attending the approximation is tremendous. The simplification is most evident if we form the equation for the Reynolds-stress deviator $(\tau_{ij} + \frac{2}{3}\rho k\delta_{ij})$ implied by the model, that is,

$$\frac{d}{dt}(\tau_{ij} + \tfrac{2}{3}\rho k\delta_{ij}) = -(P_{ij} - \tfrac{2}{3}P\delta_{ij}) + (E_{ij} - \tfrac{2}{3}E\delta_{ij}) \tag{40}$$

This equation is of first order due to the absence of diffusion terms. We should thus expect its implementation to be less difficult than that of a full Reynolds-stress transport model. This has indeed proven to be the case. As the entire formulation is empirical in its essence, the usefulness of and justification for any such approximation ultimately lies in how well the model performs in applications, and we defer to the applications of the following sections as our justification.

A few additional words regarding the absence of diffusion terms are in order. One guiding premise of this modeling effort has been to include the minimum amount of complexity while capturing the maximum amount of the physics of turbulence, with the central goal being to remove limitations imposed by the Boussinesq approximation. Most turbulence modeling researchers accept without question the commonly used approximation that triple correlation terms in the exact equation for τ_{ij} can be modeled with a gradient-diffusion approximation. Aside from the fact that using gradient-diffusion approximations to describe any aspect of turbulent mixing requires stretching the imagination a bit, it seems pointless to include such terms at the expense of elegance and mathematical complexity. This is especially true since, in most applications, the standard diffusion terms used are negligible. Ideally, the closure approximations chosen for the multiscale model implicitly include all salient effects of the triple correlation terms. To carry this discussion any further, however, violates a basic objective of this study, viz., to model the physics of turbulence rather than the differential equations.

IV. Homogeneous Turbulence

The first round of applications is to homogeneous turbulent flows. The cases selected are most of those considered in the second Stanford conference[1] and are as listed in Table 1. Most of the results submitted to the Stanford conference for the homogeneous turbulence cases could not be considered acceptable for general engineering applications. As will be shown in this section, the multiscale model performs exceptionally well for homogeneous turbulent flows. Note that in all of the homogeneous turbulence computations performed, the initial value of the specific dissipation rate ω_o has been chosen to insure a match between computed and measured turbulent kinetic energy k at the end of the computation. The average difference between the value of ω_o determined in this manner and the values recommended for use in the conference is 17%.

A. Decay of Isotropic Turbulence

Decay of isotropic turbulence is the simplest of all homogeneous turbulent flows. The case considered here is flow 0371 of the Stanford conference. The initial value of e/k has no effect on this computation. As shown in Fig. 1a, computed and measured values of k are virtually identical. This is no major surprise, however, as the ratio of β to β^* has been chosen to insure accurate simulation of this flow.

B. Effects of System Rotation

Turning now to effects of system rotation, the term in Eq. (5) proportional to ξ plays a central role. As noted earlier, this term is borrowed from the work of Bardina et al.[8] Consistent with their work, optimum agreement between model-predicted and measured turbulent energy is obtained using $\xi = 1$. Figures 1b–1d compare computed and measured turbulent energy for rotation rates of $\Omega = 0$, 20, and 80 s^{-1}. In all three cases, the initial value of the dissipation $\epsilon_o = \beta^*\omega k$ has been assumed to be 262 m^2/s^3, which corresponds to the three different dissipation rate values quoted. Again, the ratio $(e/k)_o$ has no effect on the predicted value for k. As shown, computed turbulent energies are well within the scatter of the experimental data.

C. Return to Isotropy

The least satisfactory of all the homogeneous turbulence applications in the Stanford conference were those for the return of initially anisotropic turbulence to isotropy. Figures 1e–1h compare computed and measured k, $\overline{u'^2}$, and $\overline{v'^2}$ variation with time for cases 0373A-D. Table 1 summarizes initial values used for dissipation rate $(e/k)_o$ and Re_T. As shown, model predictions differ from corresponding measured values by less than 10% for all four cases. The predicted results are sensitive to the initial value of e/k, but, as will be discussed in the next subsection, the values used are sensible.

D. Plane Strain

The two plane strain cases included in the Stanford conference differ in the value of the strain rate. Flow 0374A, corresponding to the experiment performed by Townsend,[13] has $\hat{\epsilon} = \partial w/\partial z = -\partial v/\partial y = 9.44$ s^{-1}. Flow 0374B, corresponding to the Tucker-Reynolds[14] experiment, has approximately half of this value, $\hat{\epsilon} = 4.45$ s^{-1}. In the Stanford conference, the portion of the Tucker-Reynolds experiment for which the strain rate is removed and the turbulence allowed to approach isotropy ($t > 0.4$s) was included as a return to

Table 1 Summary of homogeneous turbulence test cases

Flow ID	Description	Figure	$\omega_o(s^{-1})$	Re_T	$(e/k)_o$
0371	Decay of isotropic turbulence	1 a	512	53.5	–
0372A	System rotation; $\Omega = 0$	1 b	2980	2.0	–
0372B	System rotation; $\Omega = 20$ s^{-1}	1 c	2950	2.0	–
0372C	System rotation; $\Omega = 80$ s^{-1}	1 d	2610	2.6	–
0373A	Return to isotropy	1 e	17	6.6	0.66
0373B	Return to isotropy	1 f	47	5.0	0.86
0373C	Return to isotropy	1 g	70	9.5	0.71
0373D	Return to isotropy	1 h	72	24.2	0.64
0374A	Plane strain; $\hat{\epsilon} = 9.44$ s^{-1}	1 i	165	14.8	0.75
0374B	Plane strain; $\hat{\epsilon} = 4.45$ s^{-1}	1 j	100	32.7	0.75
0376A	Uniform shear; $\partial U/\partial y = 12.9$ s^{-1}	1 k	84	67.0	0.80
0376B	Uniform shear; $\partial U/\partial y = 48.0$ s^{-1}	1 l	86	138.0	0.80

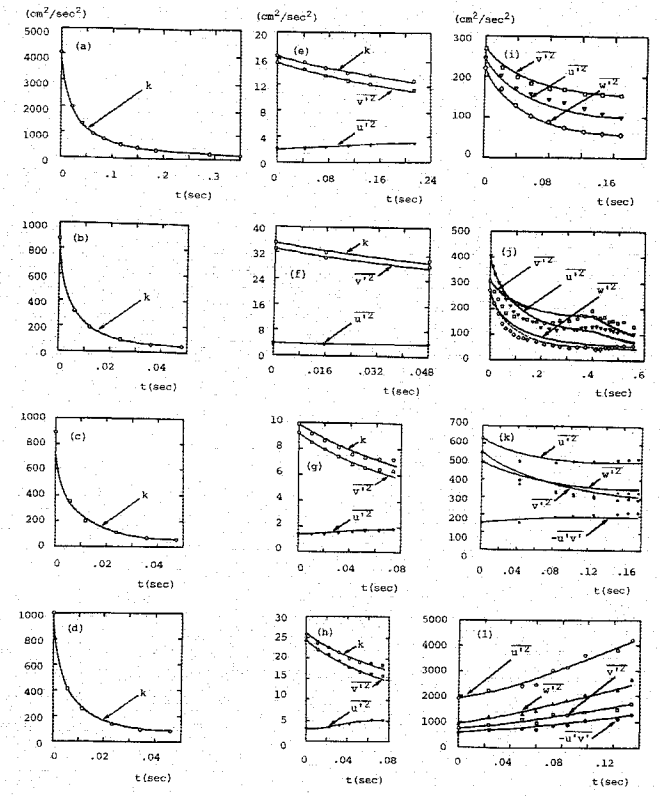

Fig. 1 Comparison of computed and measured turbulent energy and Reynolds stresses for homogeneous turbulence (———— computed, ○ ● □ △ ▽ measured).

isotropy case, flow 0373E. In the computation done in this study, flows 0374B and 0373E have been combined into a single computation.

Figures 1i and 1j compare computed and measured variations of k, $\overline{u'^2}$, and $\overline{v'^2}$ for the two cases. Just as with the wall layer, an asymptotic analysis shows that for very long times the ratio of e to k approaches a constant value of approximately 3/4 for plane strain. The Townsend case was done using an initial ratio $e/k = 3/4$. Varying the initial ratio between 1/2 and 9/10 produces less than a 15% change overall in the Reynolds stress components. Figure 1j shows the results obtained for the Tucker-Reynolds case using initial e/k ratios of 3/4 (solid curves) and 9/10 (dashed curves). As shown, the primary difference appears in $\overline{w'^2}$. Using the larger value produces closer agreement between theory and experiment. Consistent with the asymptotic analysis, by the end of the computation e/k is almost exactly 3/4, regardless of the value used for $(e/k)_o$.

Although the model has not been applied to any of the axisymmetric strain cases included in the Stanford conference, we have numerically investigated the asymptitic solution for large time. This analysis is pertinent to the return to isotropy cases discussed in the preceeding subsection because the experimental setup used by Uberoi[15] in collecting the data of cases 0373A–D first subjected the turbulence to axisymmetric strain, followed by a return to isotropy. Interestingly, the asymptotic ratio of e to k depends on the ratio of the strain rate to the initial value of ω. The asymptotic value of e/k can range from 1/2 to almost 9/10. As noted earlier, the values used in the computations for flows 0373A–D fall within this range.

E. Uniform Shear

The final applications for homogeneous turbulence are for uniform shear. The Stanford conference included two cases, flow 0376A that corresponds to the experiment by Champagne et al.[3] in which the mean shear is $\partial U/\partial y = 12.9\ \mathrm{s}^{-1}$, and flow

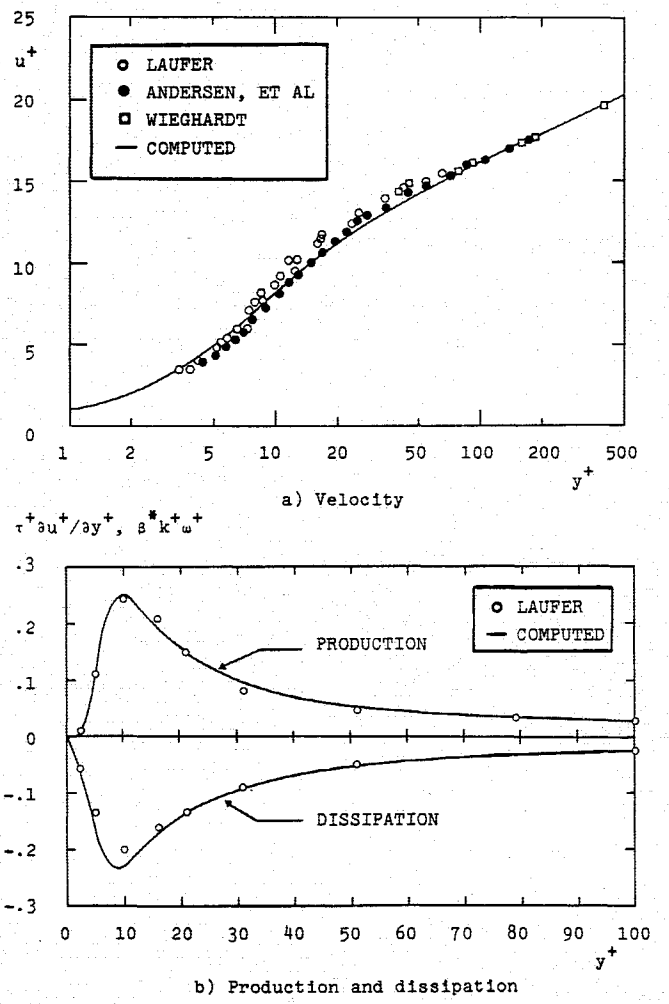

Fig. 2 Comparison of computed and measured sublayer properties for a perfectly smooth surface.

0376B that corresponds to the experiment by Harris et al.[16] in which the mean shear is $\partial U/\partial y = 48.0\ \mathrm{s}^{-1}$. Figures 1k and 1l compare computed and measured Reynolds stresses. For uniform shear, the asymptotic value of e/k for large time is 4/5. Both computations use $(e/k)_o = 4/5$.

V. Viscous Sublayer

To prepare the multiscale model for application to flows with solid boundaries, we now examine the limiting form of the model-predicted solution for the viscous sublayer. The solution exactly parallels the perturbation analysis given by Wilcox.[2] For a perfectly smooth surface, the constant in the law of the wall B is defined by

$$\frac{u}{u_\tau} = \frac{1}{\kappa}\log\frac{u_\tau y}{\nu} + B \tag{41}$$

where u_τ is friction velocity and κ is von Kármán's constant. Using the perturbation analysis procedure described by Wilcox,[2] the value of B predicted by the model depends on the value selected for the closure coefficients σ and σ^*. Using $\sigma = \sigma^* = \frac{1}{2}$ yields

$$B = 5.2 \tag{42}$$

for a perfectly smooth surface. Since this value falls well within the scatter of experimental data, this computation serves as the basis for selecting the values quoted for σ and σ^*. In addition, these results indicate that no special viscous

damping terms are needed for any of the multiscale model's closure coefficients to accommodate integration through the viscous sublayer. Figure 2 compares computed and measured[17-19] sublayer properties. As shown, differences between theory and experiment are insignificant.

VI. Boundary-Layer Applications

A. Incompressible Boundary Layers

The first case selected is the boundary layer on a flat plate for which the pressure is constant. This, and all of the steady boundary-layer computations reported in this paper, have been done with a two-dimensional or axisymmetric boundary-layer program named EDDYBL.[20] The computation extends from a plate-length Reynolds number Re_x of 1.0×10^6 to 10.9×10^6. Figures 3a and 3b compare computed and measured skin friction C_f and velocity profiles. As expected, differences between theory and experiment are almost insignificant, with the largest differences being less than 3%.

The next two cases focus on effects of adverse pressure gradient. Two cases are selected: the moderate adverse gradient case of Bradshaw[19] (case 3300) and the increasingly adverse gradient case of Samuel and Joubert[1] (flow 0141). For the Bradshaw case, Figs. 3c and 3d compare computed and measured skin friction and a velocity profile at the final station. Differences between theory and experiment are almost undetectable. For the Samuel-Joubert case, Figs. 3e–3g compare computed and measured flow properties. As shown, computed and measured skin friction differ by less than 3%, velocity profiles are nearly identical, and Reynolds shear-stress profiles differ by less than 7%.

B. Compressible Boundary Layers

As a first test of the multiscale model for compressible flows, we consider flows 8101 and 8201 of the second Stanford conference.[1] Flow 8101 addresses the adiabatic wall case with freestream Mach numbers ranging from 0 to 5. For each Mach number, computation begins at $Re_x = 1.0 \times 10^6$ and continues to the point where momentum-thickness Reynolds number is 10,000. Figure 4a compares computed ratio of skin friction to the incompressible value C_{fo} with the correlation developed by Rubesin for the second Stanford conference. Differences between computed ratios and correlated values are trivial.

Flow 8201 focuses on effects of surface temperature on flat-plate skin friction. For this round of computations the freestream Mach number is 5; the ratio of surface temperature to the adiabatic wall value ranges from 0.2 to 1.0. Again, computation begins at $Re_x = 1.0 \times 10^6$ and terminates when momentum-thickness Reynolds number is 10,000. Figure 4b compares the predicted ratio of C_f to the incompressible value with Rubesin's correlation for the range of surface temperatures considered. Differences between predicted values and correlated values nowhere exceed 4%.

The final compressible boundary-layer application is for a Mach 4, adiabatic-wall boundary layer subjected to an adverse pressure gradient. The data are attributed to Zwarts and correspond to flow 0842 of the second Stanford conference. Figure 5 presents results of the computation. As shown, computed and measured skin friction C_f, shape factor H, and momentum thickness θ differ by less than 8%.

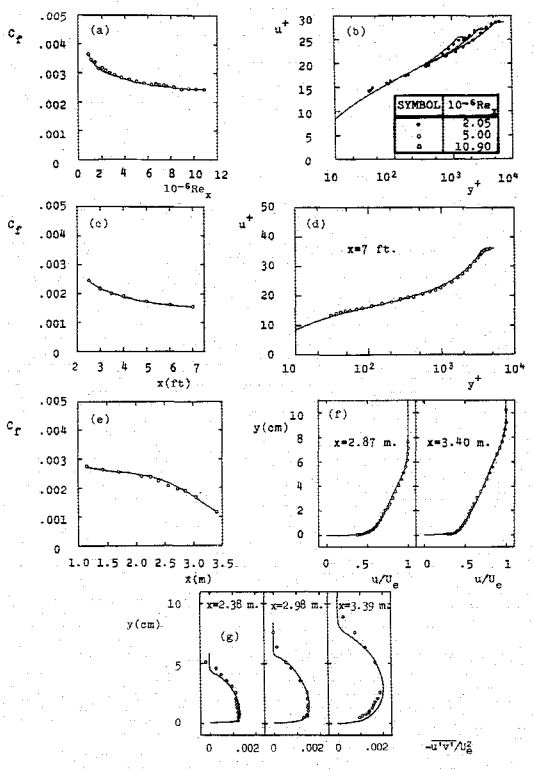

Fig. 3 Comparison of computed and measured skin friction and profiles for incompressible boundary layers (——— computed, ○ ● □ measured).

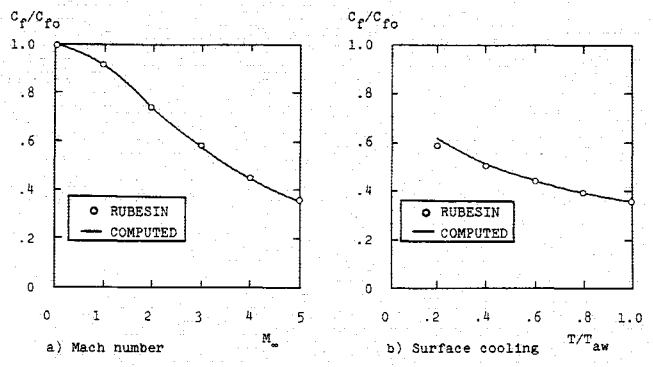

Fig. 4 Comparison of computed and measured effect of freestream Mach number and surface cooling on flat-plate boundary-layer skin friction.

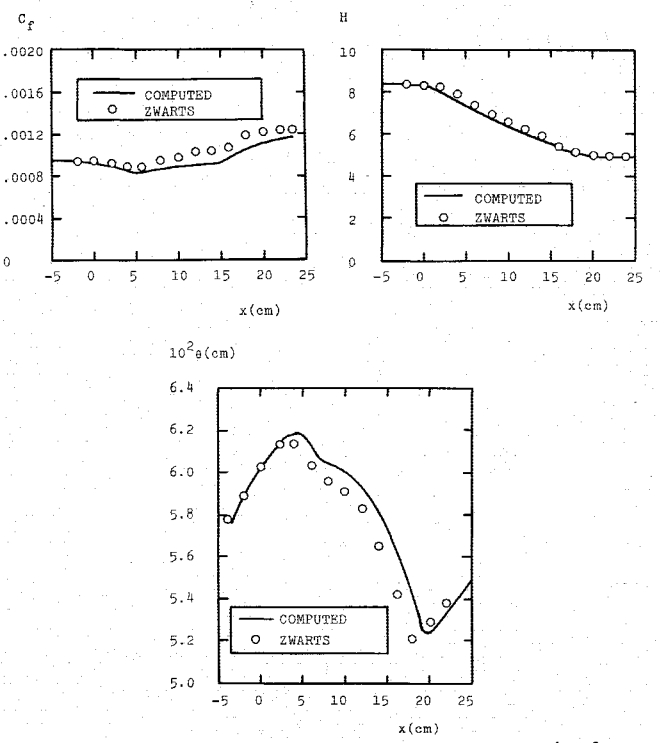

Fig. 5 Comparison of computed and measured properties for a Mach 4 boundary layer with adverse pressure gradient.

C. Unsteady Boundary Layers

The final round of applications is for incompressible, unsteady turbulent boundary layers. These flows pose a difficult challenge to the model because many complicated frequency-dependent phenomena are generally present, including periodic separation and reattachment.

1. Cases Analyzed

To test the model equations for unsteady boundary layers, we have simulated the experiments performed by Jayaraman et al.[21] In these experiments, a well-developed steady turbulent boundary layer enters a test section that has been designed to have freestream velocity that varies according to

$$U_e = U_o\{1 - ax'[1 - \cos(2\pi ft)]\}$$

$$x' = (x - x_0)/(x_1 - x_0) \tag{43}$$

The quantity x' is the fractional distance through the test section where x_0 and x_1 are the values of streamwise distance x at the beginning and end of the test section, respectively.

Thus, an initially steady equilibrium turbulent boundary layer is subjected to a sinusoidally varying adverse pressure gradient. The experiments were performed for low and high amplitude unsteadiness characterized by having $a \doteq 0.05$ and 0.25, respectively. For both amplitudes, experiments were conducted for five frequencies ranging from $f = 0.1$ to 2.0 Hz. The computations simulate nine of the experiments, including all five of the low-amplitude cases and all but the lowest frequency case for high amplitude. Complete details about the numerical method, finite-difference grids, and other pertinent computational details are given by Wilcox.[22]

2. Numerical Considerations

a) Numerical algorithm. The numerical algorithm used for the computations is an unconditionally stable implicit marching method. The scheme is second-order accurate in the direction normal to the surface. For stability, particularly through separation, the computational procedure uses upwind differencing for the streamwise convection terms. Although the algorithm is unconditionally stable, the presence of source terms in the turbulence model equations makes the equations sufficiently stiff to preclude using a streamwise Courant number $C_x = U\Delta t/\Delta x$ in excess of approximately 0.6. By contrast, the boundary-layer computations are stable with a viscous Courant number $C_y = 2\nu\Delta t/(\Delta y)^2$ in excess of 600.

Integration through separation is accomplished by computing the streamwise convective term in the momentum equation according to

$$u\frac{\partial u}{\partial x} = \max[0,u]\cdot\frac{\Delta u}{\Delta x} \tag{44}$$

where $\Delta u/\Delta x$ is the finite-difference approximation to $\partial u/\partial x$. In other words, on regions of reverse flow we set the streamwise convective term to zero. This is the procedure first implemented by Reyhner and Flugge-Lotz.[23]

b) Data reduction. In order to compare computed and measured flow properties, we must decompose any flow property $y(x,t)$ in terms of three components, that is,

$$y(x,t) = \bar{y}(x) + \tilde{y}(x,t) + y'(x,t) \tag{45}$$

where $\bar{y}(x)$ is the long-time averaged value of $y(x,t)$, $\tilde{y}(x,y)$ is the organized response component due to the imposed unsteadiness, and $y'(x,t)$ is the turbulent fluctuation. In order to extract the quantities presented in graphical form by Jayaraman et al., we first note that what the program computes is the phase-averaged component $\langle y(x,t)\rangle$ defined by

$$\langle y(x,t)\rangle = \bar{y}(x) + \tilde{y}(x,t) \tag{46}$$

Jayaraman et al. expand $\langle y(x,t)\rangle$ in a Fourier series according to

$$\langle y(x,t)\rangle = \bar{y}(x) + \sum_{n=1}^{\infty} A_{n,y}(x)\cos[2n\pi ft + \phi_{n,y}(x)] \tag{47}$$

Velocity profile data, for example, are presented by Jayaraman et al. in terms of $\bar{u}(x)$, $A_{1,u}(x)$, and $\phi_{1,u}(x)$. These quantities have been extracted from the boundary-layer solution by the normal Fourier decomposition by computing the following integrals:

$$\bar{u}(x) = f\int_o^{1/f}\langle u(x,t)\rangle dt \tag{48}$$

$$A_{1,u}(x)\cos\phi_{1,u} = f\int_o^{1/f}\langle u(x,t)\rangle\cos(2\pi ft)\,dt \tag{49}$$

$$A_{1,u}(x)\sin\phi_{1,u} = -f\int_o^{1/f}\langle u(x,t)\rangle\sin(2\pi ft)\,dt \tag{50}$$

3. Results

a) Zero frequency limit. Before proceeding to the unsteady computations, we first test for consistency with a key observation made by Jayaraman et al. for the limit of zero frequency. On the one hand, they find that for the mean velocity given by Eq. (43) with $f = 0$ and $a = 0.25$, massive separation occurs in the test section. On the other hand, even at the smallest frequency for which experiments were done, when f is not zero the observed flow is much more well behaved. On the average, the boundary layer remains attached, although at some frequencies for the high-amplitude cases periodic separation and reattachment occurs.

Part of the reason for this behavior is explained by Jayaraman et al. When we set $f = 0$, the pressure gradient is given by

$$\frac{dp}{dx'} = \rho U_o^2 a(1 - ax') \qquad \text{for } f = 0 \tag{51}$$

However, because of the nonlinearity of the convective terms in the momentum equation, for any nonzero f, the mean (long-time average) pressure gradient is

$$\frac{d\bar{p}}{dx'} = \rho U_o^2 a\left(1 - \frac{3}{2}ax'\right) \qquad \text{for } f \neq 0 \tag{52}$$

The gradient for $f \neq 0$ is thus reduced (for adverse gradient, i.e., for $a > 0$) and is less likely to cause separation.

To test the model's consistency with this observation, two steady computations have been done, the first using the pressure gradient for $f = 0$ [Eq. (51)] and the second for the gradient given in Eq. (52). The computations have been performed with the steady boundary-layer program EDDYBL and with the new unsteady program. Using a value for a of 0.25, our predictions match those described by Jayaraman et al. For the pressure gradient in Eq. (51), the boundary layer separates at $x' = 0.87$. By contrast, when the pressure gradient of Eq. (52) is used, the boundary layer remains attached throughout the test section.

b) Low-amplitude cases. For each of the low-amplitude cases, computation continues for at least five and has as many as ten periods. This proves sufficient to achieve a periodic solution as determined by monitoring skin friction. Figure 6 compares computed and measured velocity profiles at $x' = 0.88$ for the five low-amplitude cases. As shown, computed mean-velocity profiles differ from corresponding measured profiles by no more than 5% of scale. Comparison of computed and measured $A_{1,u}$ profiles shows that, consistent with measurements, unsteady effects are confined to the near-wall Stokes layer at the higher frequencies ($f > 0.5$ Hz). By contrast, at the two lowest frequencies, the entire boundary

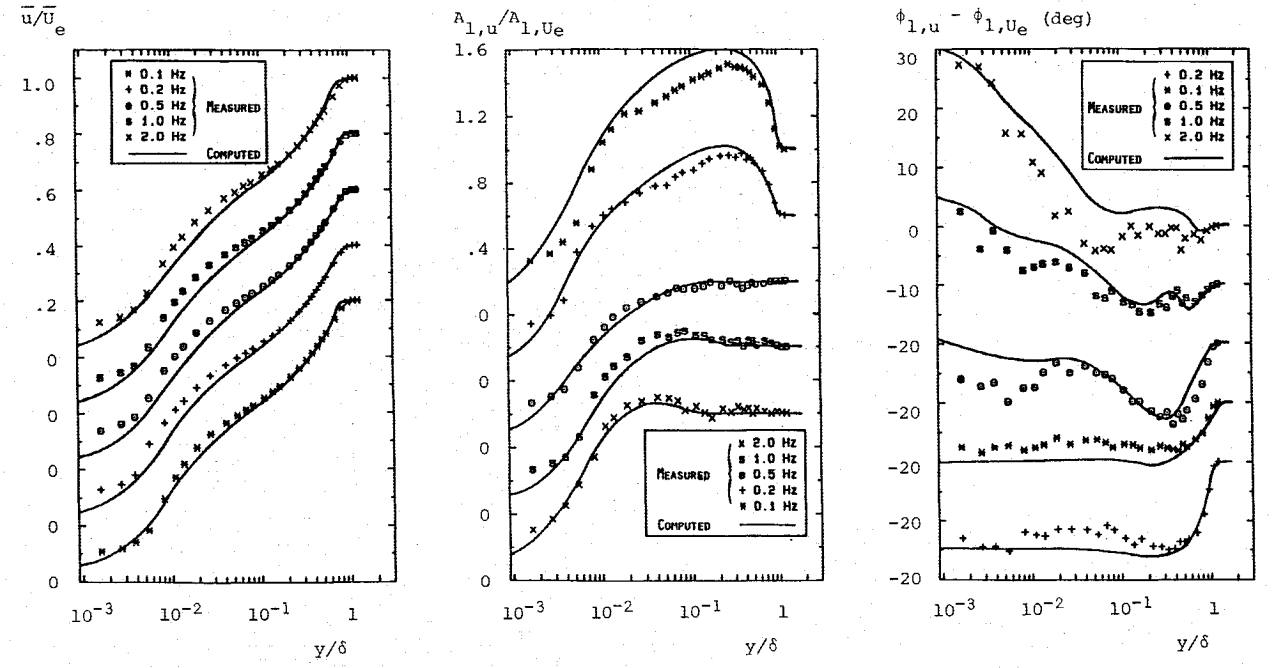

Fig. 6 Comparison of computed and measured mean velocity, $A_{1,u}$, and phase profiles; low amplitude.

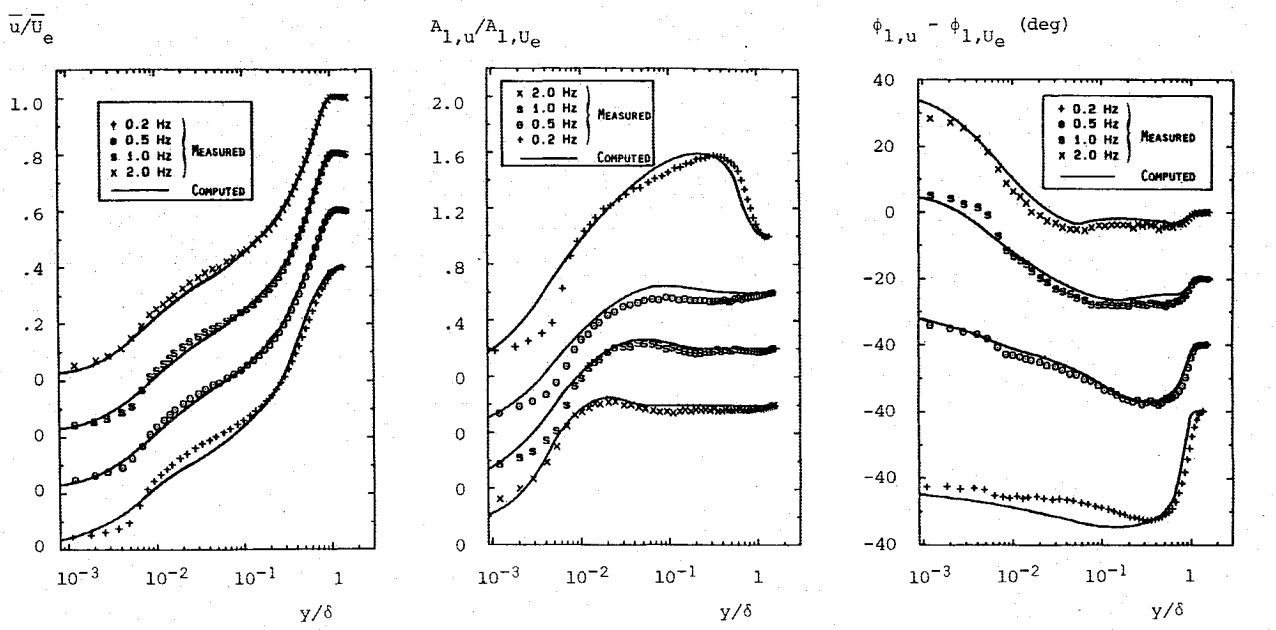

Fig. 7 Comparison of computed and measured mean velocity, $A_{1,u}$, and phase profiles; high amplitude.

layer is affected with significant amplification of the organized component occuring away from the surface. Differences between the numerical and experimental $A_{1,u}$ profiles are less than 10%. Computed and measured phase $\phi_{1,u}$ profiles are very similar with differences nowhere exceeding 5 deg.

c) High-amplitude cases. Figure 7 compares computed and measured velocity profiles at $x' = 0.94$. As with the low-amplitude cases, computed and measured $\bar{u}(x)$ profiles lie within 5% of scale of each other. Similarly, the computed $A_{1,u}$ and $\phi_{1,u}$ profiles differ from the corresponding measured profiles by less than 10%. To provide a measure of how accurately temporal variations have been predicted, Fig. 8 compares computed and measured shape factor through a complete cycle for all four frequencies. Differences between computed and measured shape factors are less than 5%.

d) k-ω model predictions. The high-amplitude cases have also been computed using the k-ω model. Results are included in Fig. 8, which shows that the k-ω and multiscale model predicitons differ by only a few percent. Although it is possible that the test cases are not as difficult as we expected, this seems unlikely in view of the wide Strouhal number range and the fact that periodic separation and reattachment are present. More likely, the k-ω model fares well because all of the cases have attached boundary layers through most of each cycle and in the mean.

VII. Summary and Conclusions

A new turbulence model has been devised that describes turbulence in terms of two energy scales. The two scales correspond to a lower and an upper partition of the turbulence

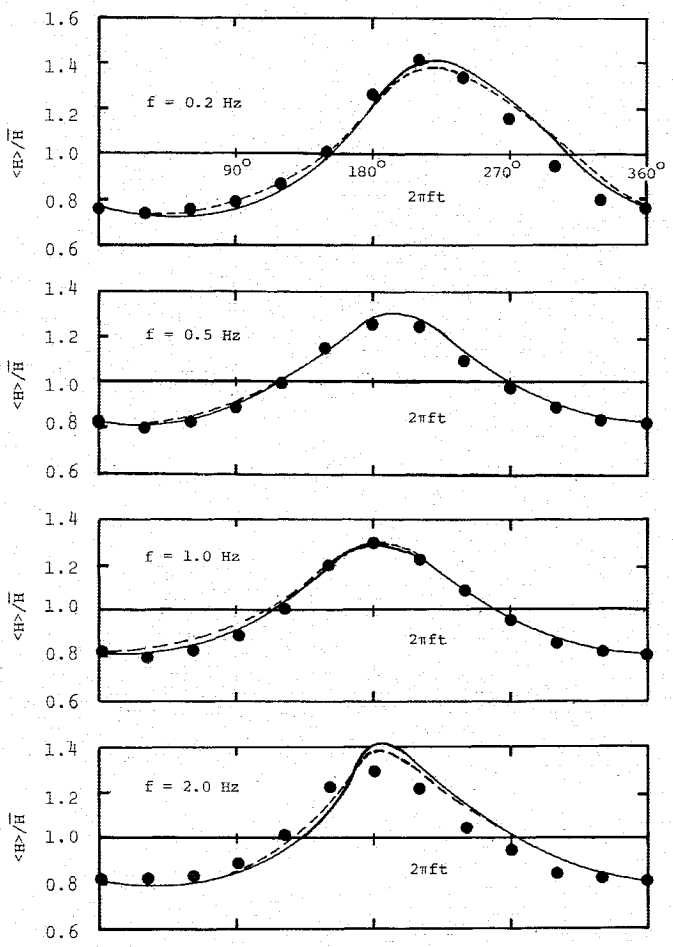

Fig. 8 Comparison of computed and measured temporal variation of shape factor for the high-amplitude cases (– – – – k-ω model, ——— multiscale model, • measured).

energy spectrum, with the upper partition corresponding to the lowest frequency eddies. Closure approximations have been designed to reflect as much as possible the physics of turbulent flow processes and to obviate limitations attending the Boussinesq approximation.

Results of the theory's application to homogeneous turbulence are very satisfactory. Virtually all of the second Stanford conference test cases have been predicted to within experimental error. Applications to the viscous sublayer indicate that, similar to the k-ω model that serves as the foundation on which the multiscale model rests, no special modifications to the closure coefficients are needed to accommodate integration through the sublayer. Results of the steady boundary-layer computations indicate the model is even more accurate than the Wilcox k-ω model for adverse pressure gradient.

From a numerical viewpoint, the new model is quite efficient, especially for the steady cases. Typically, there is only a 50% increase in computing time relative to the k-ω model for steady boundary-layer computations; the increase is typically 70% for unsteady computations.

The unsteady boundary-layer computations offer the first definitive measure of how accurately the multiscale model simulates the physics of turbulent boundary layers. For a wide range of Strouhal numbers, the multiscale model more or less duplicates the structure of a turbulent boundary layer subjected to a sinusoidally varying adverse pressure gradient. As somewhat of a surprise, the two-equation model is just as accurate for these flows.

Acknowledgment

This research has been supported by the U.S. Army Research Office under Contract DAAG-29-83-C-0003, with Dr. Robert E. Singleton as technical monitor. The original idea of developing a model based on partitioning the turbulence energy spectrum was suggested to me by Prof. John Laufer.

References

[1]Kline, S. J., Cantwell, B. J., and Lilley, G. M. (eds.), *Proceedings of the 1980-81 AFOSR-HTTM-Stanford Conference on Complex Turbulent Flows*, Vol. 1, Stanford Univ. Press, Stanford, CA, 1981.

[2]Wilcox, D. C., "Reassessment of the Scale Determining Equation for Advanced Turbulence Models," *AIAA Journal* (to be published).

[3]Champagne, F. H., Harris, V. G., and Corrsin, S., "Experiments on Nearly Homogeneous Turbulent Shear Flow," *Journal of Fluid Mechanics*, Vol. 41, Pt. 1, 1970, pp. 81-139.

[4]Wilcox, D. C. and Rubesin, M. W., "Progress in Turbulence Modeling for Complex Flow Fields Including Effects of Compressibility," NASA TP 1517, April 1980.

[5]Rodi, W., "A New Algebraic Relation for Calculating Reynolds Stresses," *Zeitschrift fuer Angewandte Mathematik und Mechanik*, Vol. 56, 1976, p. 219.

[6]Lakshminarayana, B., "Turbulence Modeling for Complex Shear Flows," *AIAA Journal*, Vol. 24, Dec. 1986, pp. 1900-1917.

[7]Johnson, D. A. and King, L. S., "A Mathematically Simple Turbulence Closure Model for Attached and Separated Turbulent Boundary Layers," *AIAA Journal*, Vol. 23, Nov. 1985, pp. 1684-1692.

[8]Bardina, J., Ferziger, J. H., and Reynolds, W. C., "Improved Turbulence Models Based on Large Eddy Simulation of Homogeneous, Incompressible Turbulent Flows," Dept. of Mechanical Engineering, Stanford Univ., Stanford, CA, Rept. TF-19, May 1983.

[9]Tennekes, H. and Lumley, J. L., *A First Course in Turbulence*, MIT Press, Cambridge, MA, 1972.

[10]Launder, B. E., Reece, G. J., and Rodi, W., "Progress in the Development of a Reynolds-Stress Turbulence Closure," *Journal of Fluid Mechanics*, Vol. 68, Pt. 3, 1975, pp. 537-566.

[11]Favre, A., "Equations des Gaz Turbulents Compressibles," *Journal de Mechanique,* Vol. 4, No. 3, 1965, pp. 361-390.

[12]Townsend, A. A., *The Structure of Turbulent Shear Flow*, 2nd ed., Cambridge University Press, Cambridge, England, 1976, pp. 66-71.

[13]Townsend, A. A., "The Uniform Distortion of Homogeneous Turbulence," *Quarterly Journal of Mechanics and Applied Mathematics*, Vol. 7, 1956, p. 104.

[14]Tucker, H. J. and Reynolds, A. J., "The Distortion of Turbulence by Irrotational Plane Strain," *Quarterly Journal of Mechanics and Applied Mathematics*, Vol. 7, 1968, p. 104.

[15]Uberoi, M. S., "Effect of Wind Tunnel Contraction of Free Stream Turbulence," *Journal of the Aeronautical Sciences*, 1956, p. 754.

[16]Harris, V. G., Graham, J. A. H., and Corrsin, S., "Further Experiments in Nearly Homogeneous Turbulent Shear Flow," *Journal of Fluid Mechanics*, Vol. 81, 1977, p. 657.

[17]Laufer, J., "The Structure of Turbulence in Fully Developed Pipe Flow," NACA TR-1174, 1952.

[18]Andersen, P. S., Kays, W. M., and Moffat, R. J., "The Turbulent Boundary Layer on a Porous Plate: An Experimental Study of the Fluid Mechanics for Adverse Free-Stream Pressure Gradients," Dept. of Mechanical Engineering, Stanford Univ., Stanford, CA, Rept. HMT-15, May 1972.

[19]Coles, D. E. and Hirst, E. A., *Computation of Turbulent Boundary Layers-1968 AFOSR-IFP-Stanford Conference*, Vol. II, Stanford Univ. Press, Stanford, CA, 1969.

[20]Wilcox, D. C., "Program EDDYBL User's Guide," DCW Industries, La Cañada, CA, Rept. DCW-R-NC-04, 1988.

[21]Jayaraman, R., Parikh, P., and Reynolds, W. C., "An Experimental Study of the Dynamics of an Unsteady Turbulent Boundary Layer," Dept. of Mechanical Engineering, Stanford Univ., Stanford, CA. TR TF-18, Dec. 1982.

[22]Wilcox, D. C., "Advanced Applications of the Multiscale Model for Turbulent Flows," AIAA Paper 87-0290, Jan. 1987.

[23]Reyhner, T. A. and Flugge-Lotz, I., "The Interaction of a Shock Wave With a Laminar Boundary Layer," *International Journal of Non-Linear Mechanics*, Vol. 3, 1968, pp. 173-199.